

Experimental investigation of amplitude dependency of dynamic characteristics in elastic and inelastic stages of reinforced concrete pier model

R. Al Sehnawi · A. Nakajima · R. Takeshima ·
H. Al Sadeq

Received: 14 March 2014 / Accepted: 10 September 2014 / Published online: 26 September 2014
© Springer-Verlag Berlin Heidelberg 2014

Abstract Structural health monitoring of existing bridges relies on vibration testing, but the free- and ambient-vibration testing techniques in current use for the determination of dynamic characteristics have a previously unknown dependency on vibration amplitude. The main purpose of this study is to investigate the dependency of the dynamic characteristics of reinforced concrete (RC) piers on the vibration amplitude in elastic and inelastic stages by applying free vibration tests to RC pier models. A series of free vibration measurements over a wide range of amplitudes were carried out with relatively small amplitude of excitation on intact models; these measurements were repeated after the models had been progressively tested to failure on a shaking table, and again after repair with carbon fiber sheets (CFS). The repair method used is one in common use for seismic repair of bridge piers: the damaged cross-section was recovered by wrapping carbon fiber sheets around the cross-section in the damaged zone, after injecting the relatively wide cracks with resin epoxy. Generally, our results indicate that overall natural frequency and damping ratio are very sensitive to the vibration amplitude level. Particularly, whenever the acceleration amplitude increases, the damping ratio significantly increases while the natural frequency slightly

decreases; which means that, when considering the dynamic characteristics of a structure, we need to pay special attention to the expected vibration amplitudes before choosing design values. We also found that the CFS repair method was effective in restoring performance characteristics of the damaged piers.

Keywords Dynamic characteristics · Amplitude dependency · RC pier model · Shaking table test · Free vibration test · Reinforced concrete seismic repair

1 Introduction

The dynamic characteristics of structures, such as the natural frequency and the damping ratio, have a significant effect on structural dynamic behavior. The actual dynamic characteristics of completed structures are inevitably different from their designated values, yet in dynamic analysis we must employ the accurate dynamic characteristics as closely as possible. To check the actual dynamic characteristics of structures, vibration measurements are typically made. Vibration measurement is also a useful technique to detect the condition of existing structures for structural health monitoring.

Previously, vibration measurements were commonly carried out on various bridge structures using large vibration-generating equipment. Although the dynamic behavior of a structure in response to significant levels of vibration can be verified by this method, vibration measurement of existing bridges is sometimes avoided due to the cost and effort required. As alternatives to generated-vibration testing, several vibration measurement methods that do not require vibration devices have been developed. These methods such as free vibration or ambient vibration testing

R. Al Sehnawi (✉) · A. Nakajima
Graduate School of Engineering, Utsunomiya University,
7-1-2 Yoto, Utsunomiya 321-8585, Japan
e-mail: dt127110@cc.utsunomiya-u.ac.jp

R. Takeshima
IHI Infrastructure Systems Co., Ltd, Tokyo, Japan

H. Al Sadeq
Department of Structural Engineering, Faculty of Civil
Engineering, Damascus University, Damascus, Syria

are used to detect structural dynamic behaviors. When using free or ambient vibration testing, however, the dependency of the dynamic characteristics on the vibration amplitude becomes a problem.

Many researchers have studied the various techniques for evaluating the dynamic characteristics of structures by collecting experimental data under different types of excitations [1–3]. Some of these studies also addressed the dependency of dynamic characteristics on response amplitude. For instance, Fukuwa et al. [4] found that the dynamic characteristics strongly depend on the response amplitude of non-structural members in a full-scale prefabricated steel building. Tamura and Suganuma [5] evaluated the amplitude dependencies with respect to natural frequency and damping ratio of three towers during strong winds. Saito et al. [6] also found that dynamic characteristics depended on amplitude in the case of the elastic stage of a steel bridge model. However, the model scale of this study was very small, and the dependency of the dynamic characteristics of reinforced concrete (RC) structures on the amplitude is not clarified in detail. In particular, the presence of damage alters the energy dissipation mechanism in RC structures, where the damage is usually associated with the formation of cracks, which also cause a degradation of the structural stiffness [7, 8]. Furthermore, the effect of the repair technique on the amplitude dependency of the dynamic characteristics is not well known. Various repair techniques have been developed by researchers and practicing engineers, to restore the function of damaged piers after an earthquake. The composite material jacket technique, using materials such as carbon fiber sheet (CFS) as jacketing, is proven effective for repairing earthquake-damaged piers [9–12], and has been applied in this study of amplitude dependency in part because of its wide use.

Vibration measurements are commonly applied in structural health monitoring, but the amplitude dependency of the dynamic characteristics of the structures is also critical to such monitoring. The main purpose of this study is to investigate the dependency of the dynamic characteristics on the vibration amplitude in elastic and inelastic stages of RC pier models by applying free vibration tests. To reach the inelastic stage, the pier model was excited to failure using the Japan Meteorological Agency (JMA) Kushiro record of the 1994 Kushiro earthquake, with peak ground acceleration (PGA) of 0.7 g. The excitations were iterative, to clarify the dynamic characteristics of RC pier models that are subjected to moderate and severe earthquake motions: we increased the seismic excitation intensity gradually to 160 % of the maximum of the Kushiro record. During the application of seismic excitation, a free vibration test was performed after each excitation iteration, to investigate the changes in dynamic characteristics during

the progression of damage. Then, the performance of the damaged pier was repaired by resin epoxy injection and CFS jacketing, and a similar test procedure was applied to the repaired pier to check the effect of the repair on the dynamic characteristics. Finally, the amplitude dependency of the dynamic characteristics of the intact, cracked, and repaired pier models were compared with each other.

2 Initial experimental model configuration, properties, and testing

2.1 Model configuration and properties

Two identical RC pier models with the same configuration were used to experimentally determine the dependency of the dynamic characteristics on the vibration amplitude. These RC pier models were designated as specimen No. 1 and No. 2. The specimens were as large as possible within the limit of the capacity of the shaking table, to maintain the proper vibration amplitude during the testing and to enlarge the range of free vibration excitation amplitude possible by hammer impact. The specimens were constructed to meet the recommendations and requirements specified by JSCE (Japan Society of Civil Engineers) standard specifications for concrete structures [13], to closely match the characteristics of existing structures. Generally, the scale effect of an RC structure is mainly related to the strength of concrete, so the dependency of the natural frequency and the damping ratio on the vibration amplitude is not affected by any scale effect.

The geometries and reinforcement details of the specimens are illustrated in Fig. 1, which shows that each experimental model is a cantilever pier consisting of a single column, cap and footing. The longitudinal reinforcement is continuous to the bottom of the footing, to provide adequate moment resistance at the base of the piers, and the connection between the piers and their caps is also effectively continuous. A concrete block was used to simulate a bridge superstructure supported by each pier [13].

As illustrated in Fig. 1, the pier cross-section was a rectangle of dimensions 100×150 mm. The clear column height was 1,500 mm. The cap cross-section was also a rectangle, of dimensions 300×350 mm and a height of 100 mm. In addition, the footing and the top weight had square cross-sections with side length of 600 mm and a height of 200 mm. In all cross-sections, the clear concrete cover was 15 mm.

Each specimen contained four longitudinal reinforcing bars of 10 mm in diameter, corresponding to a reinforcement ratio of 2.08 %. Hoops 6 mm in diameter were spaced at 100 mm throughout 300 mm from the top and

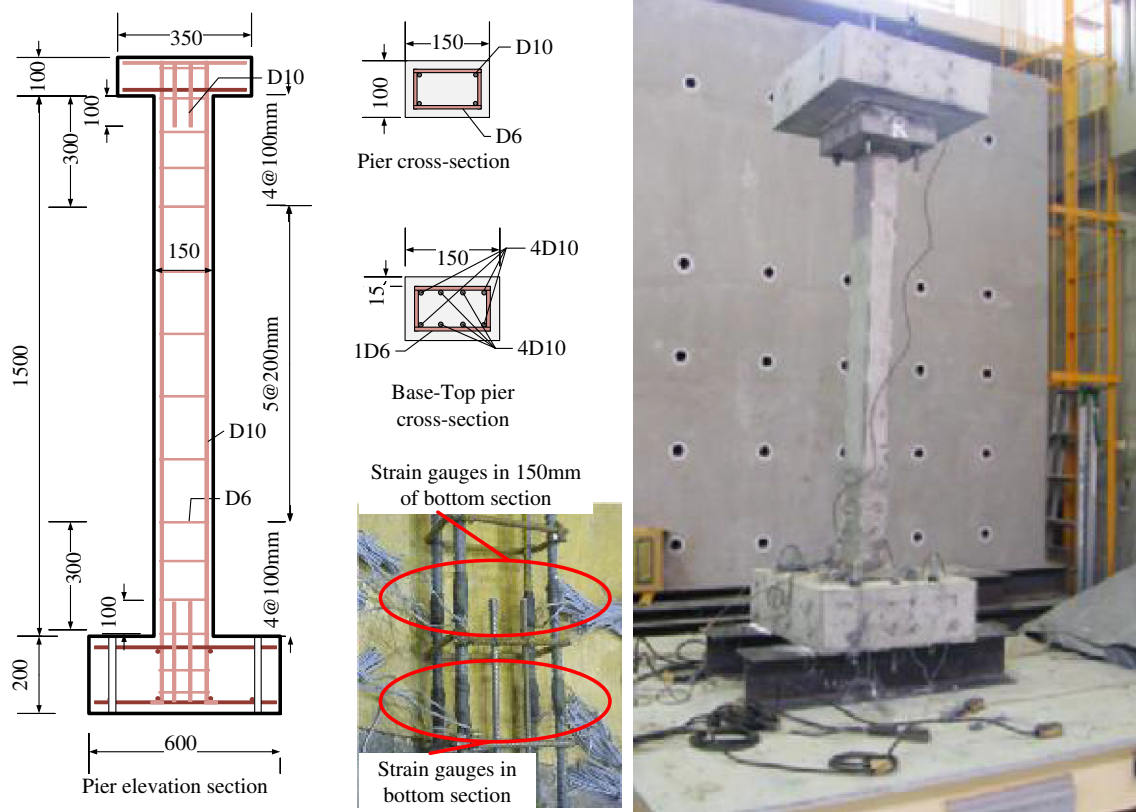


Fig. 1 Configuration of the RC pier models, and position of the strain gauges

bottom of each pier; hoops were spaced at 200 mm within the central part of the piers. Four additional reinforcement bars were added at the pier-footing connections and at the pier-caps with length of 100 mm from the connection surface to avoid cracks in the connection surface.

The yield strength of the longitudinal reinforcing bars is 401 N/mm² and the Young’s modulus of the reinforcing bars is 210 kN/mm².

For specimen No. 1, during the experimental period of 127 days, the compressive and tensile strengths of the concrete were 32.5 and 2.68 N/mm², respectively, and the Young’s modulus was 31.9 kN/mm². For specimen No. 2, during the experimental period of 155 days, the compressive and tensile strengths of the concrete were 31.8 and 2.3 N/mm², respectively, with a Young’s modulus of 29.1 kN/mm².

Strain gauges were installed on both sides of all longitudinal reinforcing bars at two positions: (1) in the bottom cross-section of the pier, and (2) at a distance of 150 mm from the top of the footing.

Figure 1 shows also the fixation of the pier footing to two steel I-girders with six bolts of 20 mm in diameter, to resist the longitudinal, transverse and rotational movement of the specimen. The additional weight simulating a bridge

superstructure was fixed to the pier cap using four bolts of 20 mm in diameter.

2.2 Free vibration test

Free vibration was excited by hammer impact at the top of the RC pier model with the additional weight. The horizontal acceleration responses were recorded by an accelerometer placed at the top of the concrete block of the pier model. The pier model oscillated around the weak axis of the cross-section. The accelerometer measured 8,192 data points per channel, resulting in a measurement period of 8.192 s for each set-up. The fixation degree of the specimen base was found by measuring the vertical acceleration responses at the top of the footing. Figure 2 shows an example of simultaneous measurement of free vibration response waveforms. Figure 2a, c shows, respectively, the time-history waveform of the measured horizontal and vertical acceleration response at the top of the pier and the footing that was subjected to large excitation amplitude, while Fig. 2b, d shows the simultaneous measurement of time-history waveform of the measured horizontal and vertical acceleration response at the top of the pier and the footing that was subjected to small excitation amplitude.

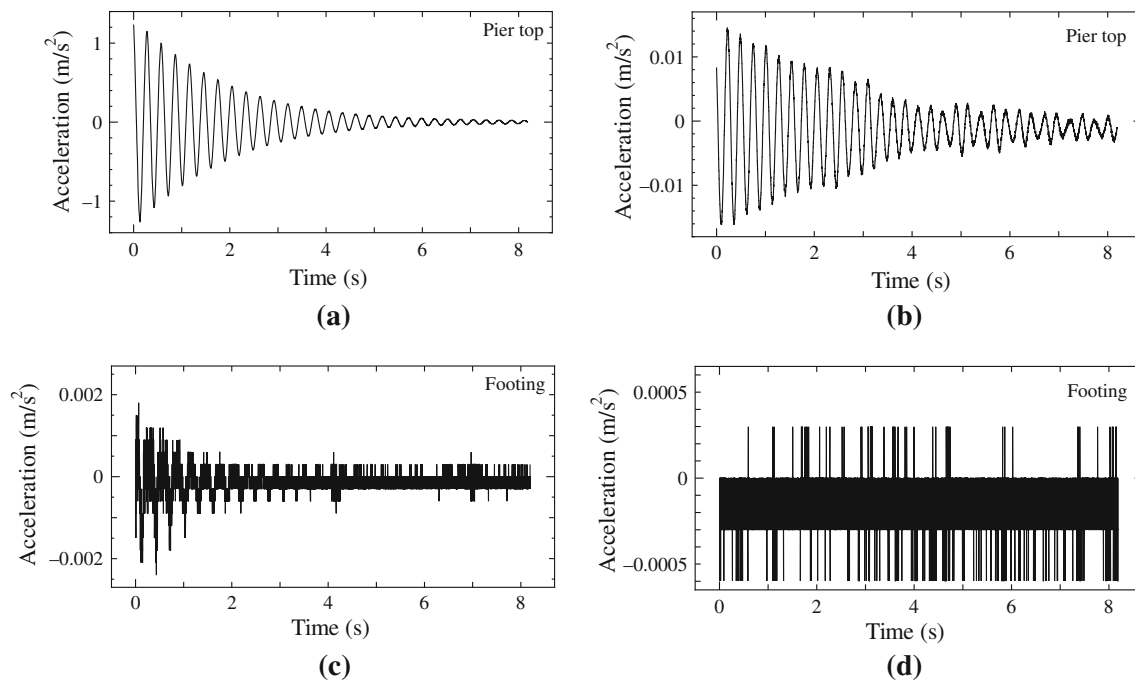


Fig. 2 Simultaneous measurements of the horizontal and vertical acceleration time-history responses, respectively, at top of the pier and footing. **a** Largest horizontal time-history response at the top of

the pier. **b** Smallest horizontal time-history response at the top of the pier. **c** Largest vertical time-history response at the top of the footing. **d** Smallest vertical time-history response at the top of the footing

Note that in Fig. 2d, an extremely small vertical acceleration at the top of the footing was revealed corresponding to the small horizontal acceleration response at the top of the pier model, whereas in Fig. 2c, a large measured vertical acceleration at the top of the footing was revealed during the large excitation amplitude. This implies that the movement of the footing is not neglected and the radiation damping occurs under large excitation of the pier. This radiation damping could be assumed as a simulation of the effect of the soil-structure interaction and energy dissipation [6].

We extracted the natural frequency of free vibration response of the pier model using a fast Fourier transform (FFT) algorithm [14, 15]. The damping ratio was identified from the filtered free decay function by fitting exponential functions to the relative maxima of these free decays [16]. Figure 3a illustrates the Fourier spectrum of the time-history acceleration response of free vibration that is shown in Fig. 2a; a band-pass filter was applied with bandwidth of 5 % above and below the natural frequency to reduce the noise effect. Note that in Fig. 3a, only one dominant frequency is observed. The relationship of the acceleration versus wave number of the peak of each cycle in the filtered waveform is shown in Fig. 3b, in which the blue and the pink lines correspond to the positive and negative exponential functions, respectively, of the filtered free decay function.

2.3 Shaking table excitations

After conducting free vibration testing on the intact specimens, we studied the influence of different damage scenarios on the dynamic characteristics of each specimen by the application of shaking table excitation to create progressive damage. The variations in the natural frequency and the damping ratio of each pier model were investigated after incurring damage at the plastic hinge zone at the pier base. To represent moderate and severe earthquake motions, each intact specimen was excited by a scaled ground motion in imitation of the 1994 Kushiro earthquake with respect to the weak axis direction of the pier model, using the JMA Kushiro record with PGA of 0.7 g. The shaking table excitation was conducted iteratively with seismic excitation intensities of 15, 20, 25, and 30 %, followed by intensity increases at 10 % increments until reaching 160 % of the Kushiro peak intensity. Finally, the specimens were repaired and these shaking table test procedures were repeated to check the effectiveness of the repair with regard to the dynamic characteristics of the specimens. Each seismic excitation was followed by a free vibration test to evaluate the changes in natural frequency and damping ratio of the specimens.

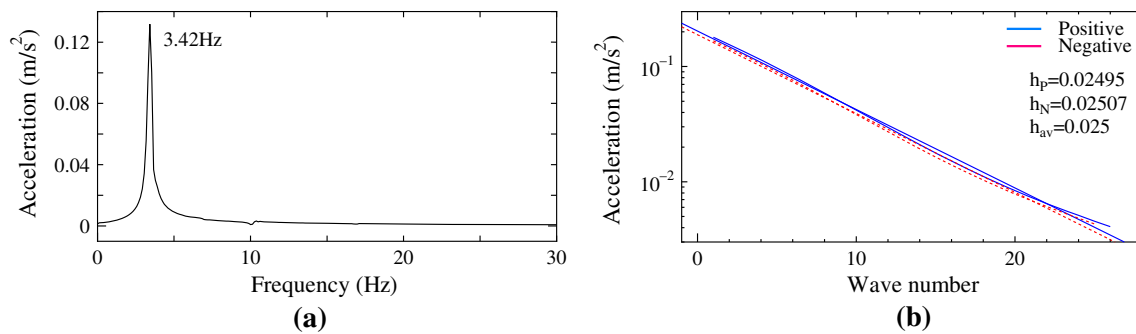
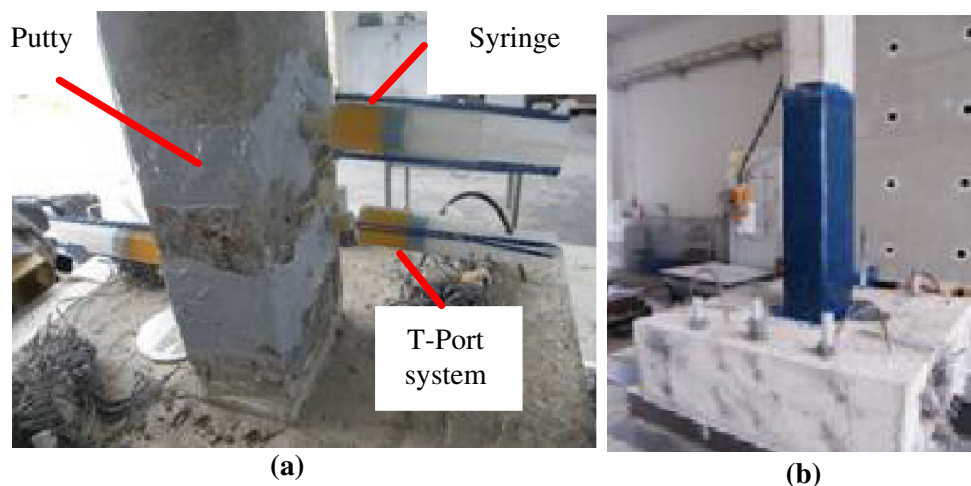


Fig. 3 a Fourier spectrum and b logarithmic decrement

Fig. 4 Crack repairs using a resin epoxy injection, and b CFS jacketing



2.4 Model damage in initial experiment

Damage progress of the specimens during shaking table excitations comprised horizontal flexural cracks. Early cracks developed close to the bottom of the pier model, within 150 mm from the top surface of the footing. At later stages of the excitation, the cracks extended into the neutral axis of the cross-section of the pier model, and horizontal flexural cracks were developed to a distance of about 300 mm from the top surface of the footing, while the concrete cover did not spall off. However, because no significant diagonal shear cracks were found, the failure mode of the specimens was identified as flexural failure [4].

3 Model repair: design, application, and testing

3.1 Summary of repair and testing

The damaged specimens were repaired by resin epoxy injection and carbon fiber sheet (CFS) jacketing. The repair procedures were similar in the two specimens and can be summarized as follows. After the surface of the cracked

concrete was cleaned of small debris, the wide cracks were injected with resin epoxy as illustrated in Fig. 4a, and putty was applied to smooth the exterior. Epoxy was also applied on the surface of the CFS sheets during wrapping of the sheets around the pier cross-section. The epoxy-impregnated sheets were tightly wrapped around the pier to ensure that there were no entrapped air pockets or fabric distortions. CFS jackets were wrapped twice, once with the fiber orientation horizontal to prevent the shear failure, and again with vertical fiber orientation to prevent the flexure-shear failure [9].

In this work, we used CFS sheets of 0.111 mm thickness, ultimate tensile strength of 3,400 N/mm², and modulus of elasticity of 245 kN/mm². Three days after application of the wrapping, the repaired specimens were tested to failure to examine the effectiveness of the repair technique.

3.2 Seismic design of carbon fiber sheet jackets

Because there are no seismic repair design guidelines available, we used the seismic retrofit guidelines for RC piers to restore confinement using CFS jacketing [17].

However, previous workers developed various experimental models to derive the design equations of bridge piers jacketed with composite materials under seismic action, and to examine the applicability to seismic repair of the design equation proposed by Priestly et al. [11] for seismic strengthening. Consensus is that the design equation for bridge pier strengthening before an earthquake could be applicable to seismic repairs after an earthquake, if the shear strength contribution of the spiral bars in the repaired piers is disregarded and 1.5 times more composite materials sheets are provided [18].

Here, to provide a design baseline of CFS jacketing for the purpose of flexural ductility enhancement and restoration of shear strength, the design equations for bridge pier strengthening before an earthquake (Eqs. 1, 6) were adopted for seismic repair design by CFS jacketing, taken according to Ogata et al. [10] and Zhiguo et al. [18]. Because the design approach and equations are detailed in Priestly et al. [11], they are not repeated here; only the pertinent final equations are provided to facilitate ease of reference.

3.3 Confinement for flexural ductility enhancement

For enhancement of the flexural ductility of a rectangular jacket with composite materials such as CFS, the maximum required compression strain ε_{cu} of the CFS is given by the following Eq. 1 [11]:

$$\varepsilon_{cu} = 0.004 + \frac{1.25\rho_s \times f_{uj} \times \varepsilon_{uj}}{f'_{cc}}, \quad (1)$$

where f'_{cc} is the compression strength of the confined concrete. The conservative value of f'_{cc} can be estimated as 1.5 times of the compression strength of concrete f'_c , f_{uj} and ε_{uj} are the ultimate stress and strain, respectively, of the jacket material, and ρ_s is the volumetric ratio of transverse reinforcement of the rectangular jacket that may be expressed as the followed equation:

$$\rho_s = 2t_j \left[\frac{b+h}{b \times h} \right] \quad (2)$$

Here, b and h are the section dimensions of the pier column and t_j is the required jacket thickness. For a more rigorous approach, the required level of transverse reinforcement ρ_s should be satisfied with Eq. 3. To avoid buckling of longitudinal reinforcement over a critical length, several hoops of a longitudinal bar should be involved in the strain hardening range of axial compression.

$$\rho_s = \frac{0.45nf_s^2}{E_{ds}E_t} \quad (3)$$

Here, $E_{ds} = 4E_sE_i/(\sqrt{E_s} + \sqrt{E_i})^2$ is the double modulus of longitudinal reinforcement at the axial stress in the bar of buckling, f_s ; E_t is the modulus of elasticity of the transverse reinforcement; E_i is elastic modulus of the longitudinal reinforcement; E_s is the secant modulus from f_s to the ultimate stress f_u ; and n is the number of longitudinal reinforcing bars. For grade SD295A reinforcement, taking $f_s = 540 \text{ N/mm}^2$ corresponding to an axial compression strain of 4 % and assuming that E_t is the elastic value of 210 kN/mm^2 , E_{ds} is found to be 34.365 kN/mm^2 , thus the volumetric ratio can be expressed by Eq. 4:

$$\rho_s = 0.0000182n \quad (4)$$

This equation is based on equilibrium of the longitudinal bar under the P - Δ effects of an assumed displaced shape and the elastic restraining forces of the hoops. As a consequence, in the absence of definitive analysis describing the interaction between confinement and buckling resistance, it is recommended that the amount of transverse reinforcement required to restrain buckling be increased by 50 % above that given by Eq. 5:

$$\rho_s = 0.0000275n \quad (5)$$

Because the typical value of ε_{cu} ranges from 0.012 to 0.05 [11], here we have assumed ε_{cu} to be 0.012. After substituting into Eq. 1, the volumetric ratio is found to be $\rho_s = 0.0066$, which is satisfied with Eq. 5 of $\rho_s = 0.000109$ for $n = 4$. The thickness of CFS could be subtracted from Eq. 2, after substituting the value of the volumetric ratio. Consequently, the solution would be $t_j = 0.198 \text{ mm}$; which means, two carbon fiber sheets with thickness of $t_j = 0.111 \text{ mm}$ are required.

3.4 Restoring shear strength

The required jacket thickness for restoring shear strength for rectangular columns is determined as in [11, 19]:

$$t_j = \frac{\frac{V^0}{\phi_s} - (V_c + V_s)}{\pi/2 \times 0.004 \times E_j \times 2[bh/b + h]}, \quad (6)$$

where ϕ_s is the shear capacity reduction factor, assumed to be 0.85; E_j is modulus of elasticity of the carbon fiber sheet; and V_c is shear capacity contributions related to concrete. Because the thin cracks inside the core are not repairable, V_c was neglected. V_s is shear strength provided by hoops, assumed to be zero. V^0 is the column shear demand based on full flexural over-strength in the potential plastic hinge zone. Here, V^0 is calculated from measured strains during the shaking table test with 50 % of the Kushiro record excitation. In this test, the strain value $\varepsilon = 1,174 \times 10^{-6}$. Thus, the shear strength could be calculated from:

$$V^0 = \frac{\varepsilon \times EI}{y \times h}, \quad (7)$$

where E is the modulus of elasticity of concrete; I is the second moment of inertia; y is the distance from the cross-section edge to the neutral axis; and h is the pier height. The increase in shear strength in the section is achieved by constraining the opening of inclined cracks, where the loss of aggregate interlock within these cracks through limiting the column dilation in the loading direction is less than 0.4 % [11].

After calculating V^0 , the required thickness t_j becomes 0.046 mm; thus, one carbon fiber sheet with thickness of 0.111 mm is applied. This thickness is also satisfied with the condition of the applicability to seismic repair of the design equation proposed by Priestley et al. [11] for seismic strengthening. Therefore the shear strength contribution of the spiral bars in the repaired piers is disregarded, and 1.5 times more CFS sheets are required [18].

3.5 Extent of jacket for confinement

The recommended minimum length of the region of the column to be confined for provision of enhanced ductility is 37.5 % of the distance from the critical section [11]. Here, the plastic hinge length of the pier model is about 300 mm; hence, the required jacket length should be 500 mm.

Consequently, the plastic hinge zones of the specimens were wrapped with three layers, having repairing length of 500 mm of CFS and an overlap length of 100 mm. Two layers were wrapped with vertical fiber orientation to restore the flexural ductility, and one layer was wrapped with horizontal fiber orientation for restoring the shear strength. Lastly, the repaired specimens were tested to examine the effectiveness of the repair technique on the dynamic characteristics.

3.6 Response on shaking table test

To elucidate the damage effect on the dynamic characteristics, specimens No. 1 and No. 2 were tested to failure both before and after repair, by applying shaking table tests. The seismic behavior of the repaired specimens was also evaluated and compared to the seismic behavior of the intact specimens. An example of cracks in the damaged specimens is depicted in Fig. 5a. We observed that the crack size increased corresponding to gradual increase of the excitation amplitude, until crack width exceeded about 2.0 mm around the pier perimeter. Hairline vertical cracks were also observed at the plastic hinge zone within 300 mm from the bottom of the pier cross-section, though the concrete cover did not spall off. Figure 5b shows a

repaired specimen; note the existence of flexural cracks within a distance of about 150 mm from the top of the CFS, while no cracks appeared on the surface of CFS.

From the shaking table test results, Fourier spectra of the acceleration time-history responses were derived by applying FFT analysis. Figure 6 shows examples of the time-history waveform of the acceleration responses at the top of the repaired specimen No. 2 subjected to Kushiro input ground motion, scaled (a) to 10 % and, (b) to 160 %. The related frequency domain representations are shown in Fig. 6c, d.

As illustrated in Fig. 6c, in the frequency domain representation of the acceleration response of the pier models under Kushiro input ground motion scaled to 10 %, at least four dominant frequency components, located at 3.09, 3.25, 3.36 and 3.54 Hz, are clearly seen. Within these dominant frequency components, the largest dominant frequency is located at 3.54 Hz. On the other hand, Fig. 6d shows the frequency domain representation of the acceleration response of the pier models under Kushiro input ground motion scaled to 160 %, and at least four dominant frequency components, located at 1.95, 2.1, 2.60 and 2.75 Hz, are also clearly seen, the largest one located at 2.1 Hz.

We observed that increasing seismic excitation corresponds to moving the dominant frequency to a lower frequency region. We attribute this to the degradation of the pier model stiffness caused by the damage sustained. The natural frequency of free vibration test after each seismic excitation, and the dominant frequency of the acceleration response (scaled Kushiro excitation) of the intact and repaired specimens No. 1 and No. 2 are illustrated in Fig. 7a, b, in which the natural and dominant frequency versus the seismic excitation intensity relationships were denoted to clarify the reduction of natural and dominant frequency of the specimens. The solid and open circles in the figures correspond to the natural frequency and dominant frequency, respectively. The black circles represent intact specimens, and the red circles represent repaired specimens.

Note that the dominant frequency derived from seismic excitation is not equal to the natural frequency derived from free vibration seen in Fig. 7. This is due to the effects of the input excitation frequency characteristics on the output response. Figure 7a, b also confirms a decrease in the dominant frequency corresponding to the increase of seismic excitation intensity in all cases. This could be referred to the presence of cracks that caused deterioration of the pier models in the plastic hinge zone.

To clarify how much the natural and dominant frequency have changed in each case, the range of the frequency changes and the ratio of frequency reduction of the original and repaired specimens No. 1 and No. 2 are shown in Table 1. The reduction ratio is defined as the ratio of

Fig. 5 Cracks **a** in the plastic hinge zone of the pier model, and **b** at the top of the CFS wrapping of the repaired pier model. **a** Cracks in original specimen, **b** cracks in repaired specimen

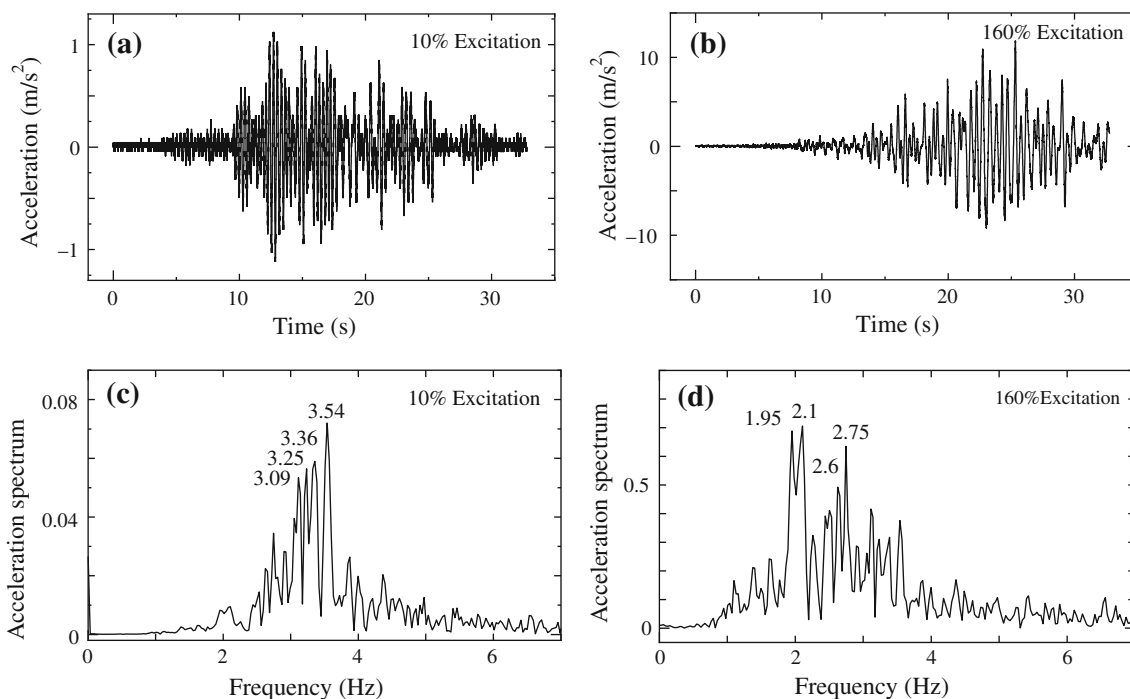
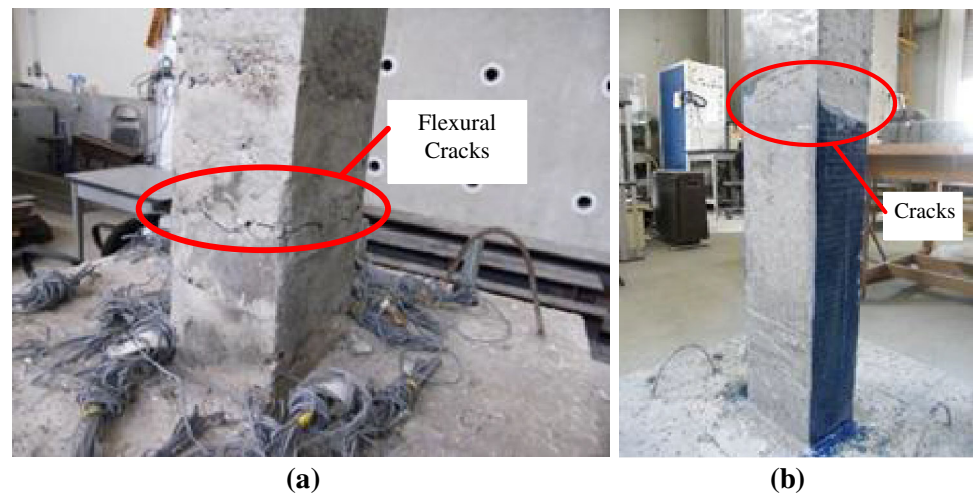


Fig. 6 Time history of the acceleration response of specimen No. 2 subjected **a** to 10 % and **b** to 160 % of Kushiro seismic excitation, and the corresponding Fourier spectra at **c** 10 % excitation and **d** 160 % excitation

extracting the frequency of the cracked specimen under 160 % of Kushiro excitation from the frequency of the intact specimen. Table 1 reveals that a decrease of the natural frequency corresponds to degradation of the pier model stiffness caused by the damage sustained. Note that the reduction ratio of frequency of both the intact specimens is remarkably larger than the repaired specimen No. 2.

The changes in the damping ratio, derived from the free vibration test after each seismic excitation with respect to seismic excitation intensities, are shown in Fig. 7c, d. Black

and red solid circles correspond to the dependency of the damping ratio of the intact (black circles) and repaired (red circles) specimens on the seismic excitation intensities. Although the increase of the excitation amplitude increases the amount of damage which causes higher damping ratio, Fig. 7c, d shows a large scatter of damping ratios based on measuring free vibration data that followed each seismic excitation. This scattering could be attributed to the difficulties of applying a similar hammer impact in the free vibration test that follows each seismic excitation. The acceleration

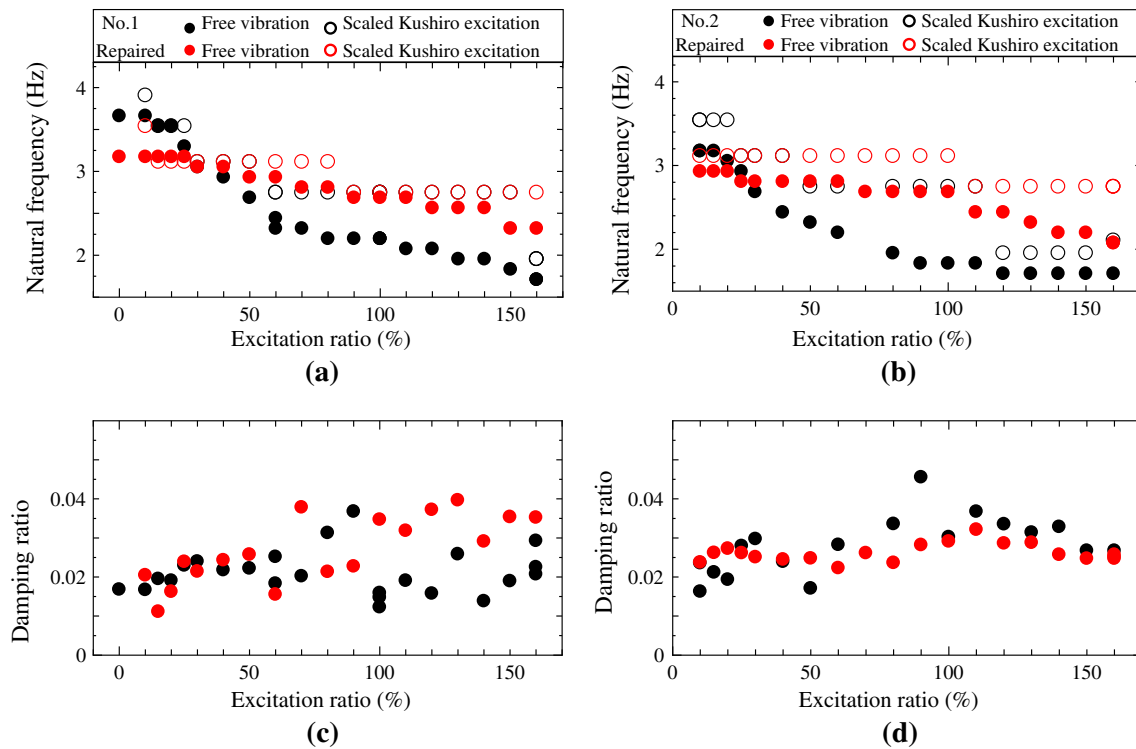


Fig. 7 Seismic excitation intensity of the scaled Kushiro earthquake versus **a** natural frequency and **c** damping ratio of specimen No. 1, and **b** natural frequency and **d** damping ratio of specimen No. 2. **a** Specimen no.1, **b** specimen no.2, **c** specimen no.1, **d** specimen no.2

Table 1 Natural and dominant frequency changes and their reduction ratio (in parentheses) of original and repaired specimens No. 1 and No. 2 during seismic excitation test

Specimen name	Natural frequency during free vibration test (%)	Dominant frequency during seismic excitation test (%)
No. 1		
Original specimen	3.66–1.71 (53)	3.9–1.95 (50)
Repaired specimen	3.17–2.32 (27)	3.54–2.75 (22.5)
No. 2		
Original specimen	3.17–1.71 (56)	3.54–2.11 (40.5)
Repaired specimen	2.93–2.08 (29)	3.11–2.75 (12)

amplitude of the free vibration was small and uneven in the range of (0.22–0.5) m/s², and the damping ratios on specimens with cracks are also affected by the energy dissipation around the crack and the radiation damping at the fixation of the pier.

3.7 Strain time-history response

Local strain time-history response characteristics were investigated to evaluate the behavior of the longitudinal reinforcement. The strain time-history response was evaluated at the plastic hinge zone near the base of the pier model, using data from the strain gauges installed at the

bottom cross-section of the pier and at a distance of 150 mm from the top of the footing.

In the strain time-history response, yield strain is defined as the strain corresponding to yield strength divided by elastic modulus of reinforcing bar, while the tensile strain is the strain corresponding to concrete tensile strength divided by elastic modulus of concrete. Examples of the strain time-history response of the original specimen No. 1 subjected to 15, 100, 150 and 160 % of the seismic excitations of the Kushiro record are shown in Fig. 8a. Note that the strain response reached the tensile strain in the first 15 % of seismic excitation, and reached the yield strain during 100 % of seismic excitation. During application of 150 % of the seismic excitation, the strain response showed a sharp strain beyond yielding in all reinforcing bars. At 160 % of the Kushiro seismic excitation, a relatively large compression strain is observed, and this compression strain is due to the local bending of longitudinal reinforcing bars in the cracked region.

Figure 8b shows examples of strain time-history response of the original specimen No. 2 subjected to 10, 60, 100 and 110 % of the seismic excitations of the Kushiro record. Note that the strain response is larger than the tensile strain from the first 10 % of seismic excitation. During the application of 60 % of seismic excitation, the strain reached the yield strain. The strain response showed

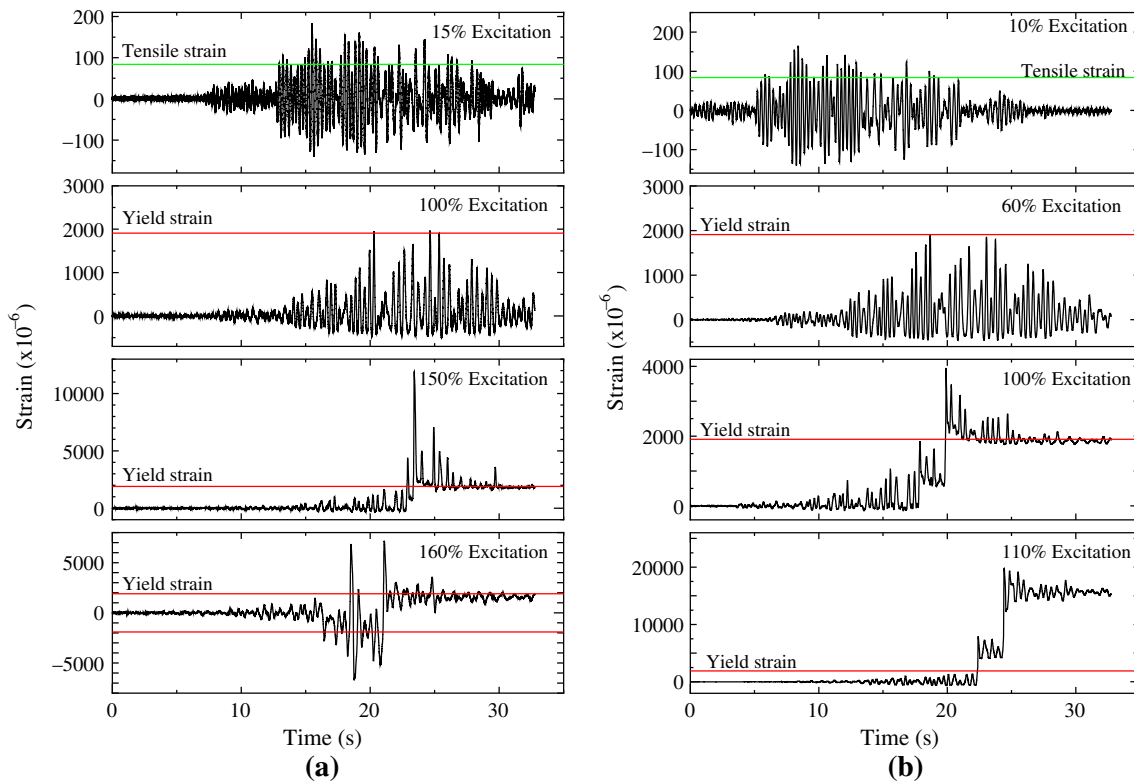


Fig. 8 Strain time-history response of steel reinforcement at pier base of original specimens No. 1 and No. 2 subjected to different seismic excitation intensities. **a** Specimen No. 1. **b** Specimen No. 2

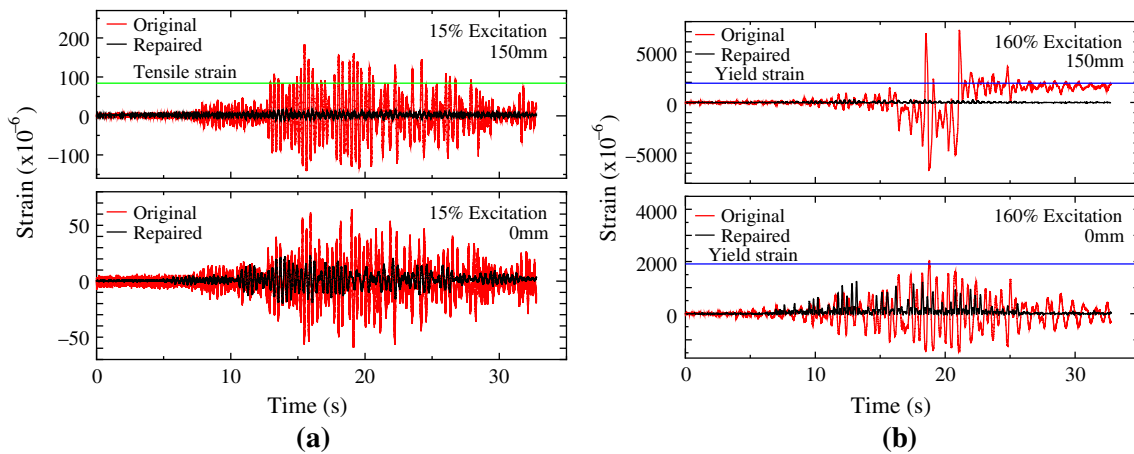


Fig. 9 Strain time-history response of steel reinforcement at pier base and 150 mm above the footing of repaired specimen No. 1 subjected to 15 and 160 % of seismic excitation intensities. **a** 15 % of Kushiro excitation. **b** 160 % of Kushiro excitation

a sharp strain beyond yielding in all reinforcing bars from 100 % of seismic excitation, and the strains gauges broke after 110 % of the excitation due to relatively large strain response.

The strain time-history responses of the repaired specimen No. 1 recorded during its testing to failure are shown in Fig. 9a for 15 % of the Kushiro seismic excitation and Fig. 9b for 160 % of seismic excitation.

Strain responses were measured in the bottom cross-section and at a distance of 150 mm from the bottom section of the original and repaired specimen No. 1. Strain time-history responses of the repaired specimen at a distance of 150 mm from the footing remained elastic at both 15 and 160 % of Kushiro seismic excitation, with values that are too small compared with those of the specimen before repair. However, the curve at 160 % of Kushiro

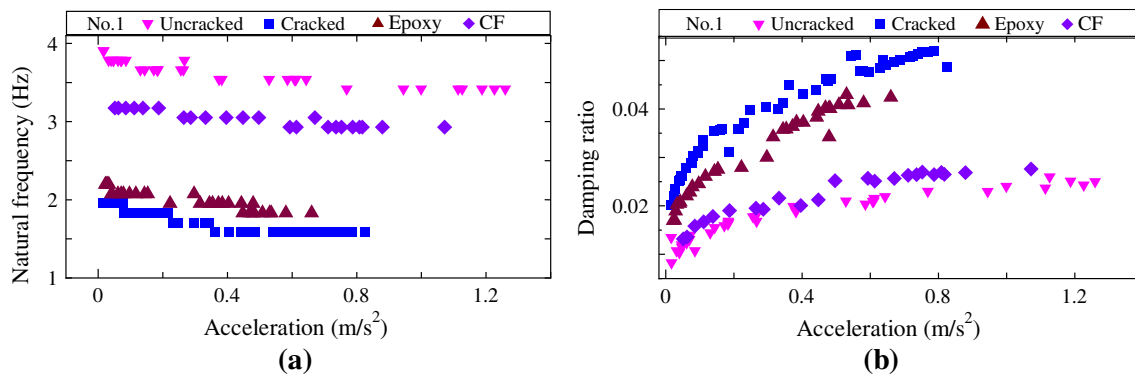


Fig. 10 **a** Maximum acceleration response versus natural frequency and **b** damping ratio of intact (pink triangles), cracked (dark blue squares), and repaired (maroon triangles, purple diamonds) specimen No. 1

excitation in the pier-footing connection region shows that the strain response values of the repaired specimen are larger than tensile strain, which may be attributed to fine cracks developed in the pier-footing connection region, even though such cracks could not be observed underneath the CFS wrapping. Significantly, the CFS-wrapped section remains essentially in the elastic range where measured at a distance of 150 mm from the footing, illustrating that repair with CFS provides piers with effective confinement [20]. In addition, before and after repair, the strain time-history response in the bottom cross-section of the pier remains in the elastic range as illustrated in Fig. 9.

3.8 Response on free vibration test

To investigate the changes in natural frequency and damping ratio under a series of different vibration levels for the intact, damaged, and repaired specimens, we conducted free vibration tests. In the intact specimens, the vibration testing was in the elastic stage of the pier model. After damage occurred in the plastic hinge zone of the specimens, i.e., in the inelastic stage of the pier model, free vibration tests were repeated. Finally, free vibration tests were applied to the repaired specimens. Figure 10a, b shows the maximum acceleration amplitude of each excitation versus the natural frequency and damping ratio relationships of each identified vibration level of the intact, cracked and repaired conditions of specimen No. 1, and Fig. 11a, b shows those relationships for specimen No. 2.

In all cases shown in Figs. 10 and 11, there is a similar tendency of the relation between natural frequency and excitation amplitude, and between the damping ratio and excitation amplitude. This tendency is observed in the elastic and inelastic stages of the pier model. In Figs. 10a and 11a, we see that increasing of the maximum acceleration amplitude leads to decreasing of the natural frequency. On the other hand, in Figs. 10b and 11b, the

damping ratio tends to increase significantly with the increasing of the maximum acceleration amplitude. The changes of the dynamic characteristics could refer to the effect of the fixation and the radiation damping at the pier base. This fact confirmed that the measured vertical acceleration increased with an increase of the excitation amplitude, as noted in Fig. 2c, d, which leads to increasing of the radiation damping.

Table 2 illustrates the maximum acceleration amplitudes recorded from hammer impact of the intact, cracked, after epoxy injection, and after CFS wrapping of the specimens No. 1 and No. 2.

Table 2, Figs. 10 and 11 together illustrate that the change range of the natural frequency and the damping ratio depends on the acceleration amplitude in all cases. Although the amplitude dependency of the natural frequency and damping ratio show similar tendencies, it is clear that when damage occurred, natural frequency decreased and damping ratio increased remarkably compared with the intact specimens.

It is also clear that the dynamic characteristics of the repaired specimens were not improved by resin epoxy injection of the wide cracks alone, which could be attributed to the low viscosity and low surface tension of the resin epoxy, plus the existence of fine cracks impossible to repair by epoxy injection. However, the stiffness of the pier model was recovered by wrapping the damaged zone of the specimens by CFS jacketing, and the natural frequency and damping ratio of the pier model were restored to values close to those of the intact specimens. The employed repair technique of applying CFS jacketing is therefore proven to have restored the dynamic characteristics successfully.

By comparing the results of the specimens No. 1 in Fig. 10 and No. 2 in Fig. 11, it is also revealed that the dependency of the natural frequency and the damping ratio on the excitation amplitude in each test stage are almost similar for both specimens.

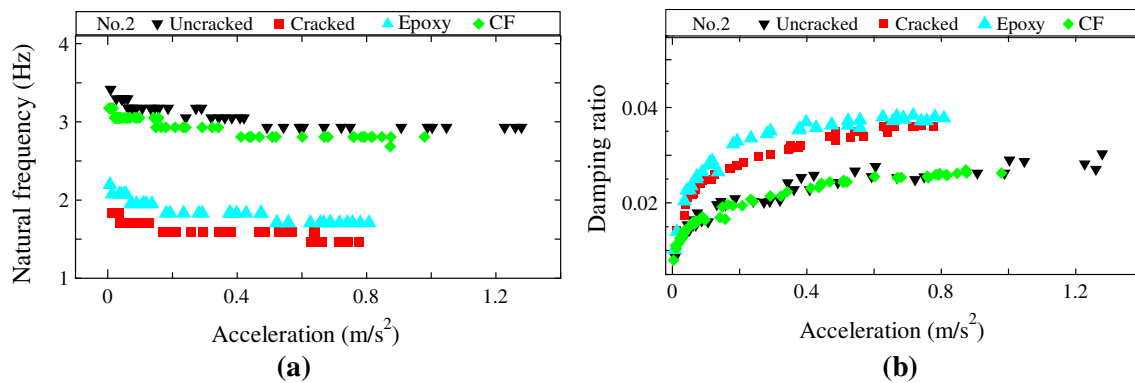


Fig. 11 **a** Maximum acceleration response versus natural frequency and **b** damping ratio of intact (*black triangles*), cracked (*red squares*), and repaired (*cyan triangles, bright green diamonds*) specimen No. 2

Table 2 Natural frequency and damping ratio of specimens No. 1 and No. 2 under free vibration test

Specimen	Acceleration (m/s ²)	Natural frequency (Hz)	Damping ratio
No. 1			
Intact	1.26–0.016	3.91–3.42	0.026–0.0083
Cracked	0.83–0.016	1.953–1.587	0.052–0.02
Epoxy injection	0.66–0.022	2.2–1.83	0.043–0.017
CFS sheet	1.07–0.05	3.17–2.93	0.028–0.013
No. 2			
Intact	1.28–0.0086	3.418–2.93	0.03–0.0087
Cracked	0.78–0.0134	1.83–1.465	0.036–0.0141
Epoxy injection	0.81–0.0067	2.2–1.71	0.038–0.01
CFS sheet	0.875–0.0038	3.17–2.81	0.027–0.008

4 Conclusions

Free vibration and shaking table tests were conducted to failure on two similar RC pier models, to determine the dependency of natural frequency and damping ratio on vibration amplitude in the elastic and inelastic stages of bridge piers. The damaged pier models were then repaired by resin epoxy injection and CFS jacketing, and retested following the same procedures conducted on the intact pier models. We conclude that:

1. The natural frequency was decreased due to the degradation of the pier model stiffness caused by damage sustained. The natural frequency reduction ratios of the original specimens during seismic excitation test are remarkably larger than the one of the damaged specimens.
2. Variation of the damping ratio corresponding to damage level caused by seismic excitation showed a scattering with respect to damage progress. This

scattering could be attributed to the difficulties of applying a similar hammer impact in the free vibration test that follows each seismic excitation. The acceleration amplitude of the free vibration was small and uneven in the range of (0.22–0.5) m/s², and the damping ratios in cracked specimens are also affected by the energy dissipation around the crack and the radiation damping at the fixation of the pier.

3. In all cases, a similar tendency of the dependency of natural frequency and damping ratio on the amplitude is observed in the elastic and inelastic stages of the pier model. Specifically, as the maximum acceleration amplitude increases the natural frequency tends to decrease, while the damping ratio tends to increase remarkably. These changes in the dynamic characteristics could be an effect of the fixation and radiation damping at the pier base that was observed from measuring the vertical acceleration at the top of the footing.

When the specimens were damaged, the natural frequency decreased and the damping ratio increased compared with the intact specimens; however, the change trend of the damping ratio is more sensitive than that of the natural frequency.

4. Finally, when considering the dynamic characteristics of a structure, we need to pay special attention to the expected vibration amplitudes before choosing design values.

Acknowledgments The authors are grateful to Structural Laboratory members of Architecture and Civil Engineering Department at Utsunomiya University, especially Dr. Y. Suzuki, for their help during the preparation of specimens. Also we are grateful to Mr. A. Kobayashi of Composites Company, Nippon Steel and Sumikin Materials Co., Ltd for providing carbon fiber sheets materials.

References

- Celebi M, Phan LT, Marshall RD (1993) Dynamic characteristics of five buildings during strong and low-amplitude motions. *Int J Struct Des Tall Build* 2:1–15
- Peeters B, Ventura CE (2003) Comparative study of modal analysis techniques for bridge dynamic characteristics. *Mech Syst Signal Process* 17(5):965–988
- Takeshima R, Al Sehnawi R, Nakajima A, Nakamura S, Yokokawa H (2014) Study on change of vibration property of bridge structure with RC Pier in different vibration level. *J Jpn Soc Civ Eng, Ser. A1 (Structural engineering and earthquake engineering (SE/EE))* (in printing)
- Fukuwa N, Nishizaka R, Yagi S, Tanaka K, Tamura Y (1989) Field measurement of damping and natural frequency of an actual steel-framed building over a wide range of amplitudes. *J Wind Eng Ind Aerodyn* 59:325–347
- Tamura Y, Suganuma S (1996) Evaluation of amplitude-dependent damping and natural frequency of buildings during strong winds. *J Wind Eng Ind Aerodyn* 59:115–130
- Saito T, Nakajima A, Takeshima R, Al Sehnawi R (2013) Experimental investigation on vibrational property change of bridge model under various input level. *J Struct Eng* 59A: 261–271 (in Japanese)
- Egba Ernest I (2012) Detection of structural damage in building using changes in modal damping mechanism. *IJEMS* 3(3): 250–255
- G. Zafra R, Kawashima K, Sasaki T, Kajiwara K, Nakayama M (2013) Seismic performance of a full-scale polypropylene fiber reinforced cement composite bridge column based on E-Defense shake-table experiments. *Proceedings of the international symposium for bridge earthquake engineering in honor of retirement of Professor Kazuhiko Kawashima, Tokyo, Japan*
- Kawashima K (2000) *Seismic design and retrofit of bridges*, 12WCEE
- Ogata N, Maeda Y, Ando H (1994) Carbon fiber strengthening of existing bridges. 2nd US-Japan workshop on seismic retrofit of bridges, pp321–333, Report no. UCB/EERC 97-9, EERC, UCB, CA, USA
- Priestley M.J.N, Seible F, Calvi G.M (1996) *Seismic design and retrofit of bridges*. TG300.P64 1996
- Wakui H, Matsumoto N (1997) Seismic retrofit of railway bridges by means of carbon fiber. *Civil Eng* 82:10–12
- Concrete Committee, JSCE (2007) *Standard specifications for concrete structures* (in Japanese)
- Committee of structural engineering, JSCE (2000) *Guidelines for bridge vibration monitoring* (in Japanese)
- Shoji G, Kitahara J, Kojima A, Kanakubo T, Shimizu K, Sakai Y (2008) Mechanism of seismic response of a PC cable-stayed bridge subjected to a long-period seismic excitation. *Doboku Gakkai Ronbunshuu A* 64(4):982–1001
- Magalhães F, Caetano E, Cunha A, Flamand O, Grillaud G (2012) Ambient and free vibration tests of the Millau Viaduct. Evaluation of alternative processing strategies. *Eng Struct* 45: 372–384
- Vosooghi A, Saiidi MS (2013) Shake-table studies of repaired reinforced concrete bridge columns using carbon fiber-reinforced polymer fabrics. *Struct J* 110(1):105–114
- Zhiguo S, Dongsheng W, Xiuli D, Bingjun S (2011) Rapid repair of severely earthquake-damaged bridge piers with flexural-shear failure mode. *Earthq Eng Eng Vib* 10(4):553–567
- Walker R, Karbhari VM (2006) Durability based design of FRP jackets for seismic retrofit. *COMPOSITE 2006 convention and trade show*. American Composites Manufacturers Association, Arlington
- Lee DH, Park J, Lee K, Kim BH (2011) Nonlinear seismic assessment for the post-repair response of RC bridge piers. *Sci Direct, Compos: part B* 42:1318–1329